Transient Response of Two-Layer Slot Coating Flows to Periodic Disturbances

Danmer Maza and Marcio S. Carvalho
Dept. of Mechanical Engineering, Pontificia Universidade Catolica do Rio de Janeiro, Rio de Janeiro, RJ 22453-900, Brazil

DOI 10.1002/aic.14734
Published online February 8, 2015 in Wiley Online Library (wileyonlinelibrary.com)

Coating uniformity requirement is becoming more severe as new products come into the market. Coating processes have to be designed not only based on the steady-state operation but also taking into account how the flow responds to ongoing disturbances on process conditions. These disturbances may lead to thickness variation on the deposited liquid layers that may be unacceptable for product performance. This study extends available transient analysis of single-layer slot coating to determine the amplitude of the oscillation of each individual coated layer in two-layer slot coating process in response to small periodic perturbation on different operating parameters. The predictions were obtained by solving the complete transient Navier–Stokes equations for free surface flows. The results show the most dangerous perturbations and how the deposited film thickness variations of each layer can be minimized by changing the geometry of the die lip and liquid viscosities. © 2015 American Institute of Chemical Engineers *AIChE J*, 61: 1699–1707, 2015
Keywords: coating flow, computational fluid dynamics, fluid dynamics, mathematical modeling

Introduction

Continuous liquid coating is the main step in the manufacturing of different functional films. For optimal performance, the film structure may have more than one layer. The most efficient way to manufacture these products is by coating all the layers at once before they are solidified.

Slot coating is one of the preferred methods to obtain a thin, uniform liquid layer over a moving substrate.[1] The coating liquid is pumped to a coating die in which the liquid is distributed across the width of a narrow slot. Exiting the slot, the liquid forms a bridge between the moving web and die lips that is bounded by an upstream and downstream gas–liquid interfaces. Slot coating process can be easily adapted for coating two different layers,[2] as shown in Figure 1. The coating die has two separate feed slots through which each layer is fed. The flow can be divided into three regions: upstream gap, midgap, and downstream gap. When both liquids are immiscible, they form an interlayer inside the coating bead. But, in several coating applications, both layers use solvents that are miscible and the apparent interface is truly an interdiffusion zone. However, because of the relatively high speed of the moving web ($\approx 1\mathrm{m/s}$) and the small length of die lip ($\approx 1\mathrm{mm}$), the residence time in the coating bead is extremely small and so is the thickness of the diffusion zone[3]; it is so thin that it can be considered as a distinct interlayer with zero interfacial tension.

Slot coating belongs to a class of methods known as premetered coating: the thickness of the deposited liquid layer is set by the flow rate fed to the coating die and the web speed and is independent of other process variables. However, the flow in the coating bead is strongly affected by the operating conditions such as coating gap, flow rate of each layer, web speed, vacuum pressure, liquid properties, and die configuration. Steady, two-dimensional flow is only possible for a certain range of parameters. The region in the space of operating parameters of a coating process at which the delivered liquid layers are adequately uniform is usually referred to as coating window. Coating window of two-layer slot coating is complex, the process is limited by different failure mechanisms that have been investigated by different researchers.

One of the important failure mechanism is related to the position of the separation point (line in three-dimensions) from which the interlayer starts. Ideally, the separation point should be lodged on the downstream corner of the midlip,[4] as shown in Figure 1, but it can transit from one corner to the other as operating condition changes.[5,6] Thus, the interlayer and the top liquid layer can invade the midgap region, accompanied by dangerous turn-around flow and sometimes by the appearance of microvortex. Nam and Carvalho[7] examined, by both flow visualization and Navier–Stokes theory, the location of the interlayer separation point along the mid die lip as the operating conditions change. They found that the location of the separation point is a strong function of the bottom-layer flow rate and almost insensitive to the other operating parameters. The midgap invasion, the movement of the separation point from the downstream corner to the upstream corner of the midlip, appears when the bottom-layer thickness is bellow 1/3 of the coating gap.

Even if the separation point is located at the downstream corner of the midlip, coating defects associated with instabilities on the interlayer may occur. Yih[8] have shown that

Correspondence concerning this article should be addressed to M. S. Carvalhoa at msc@puc-rio.br.

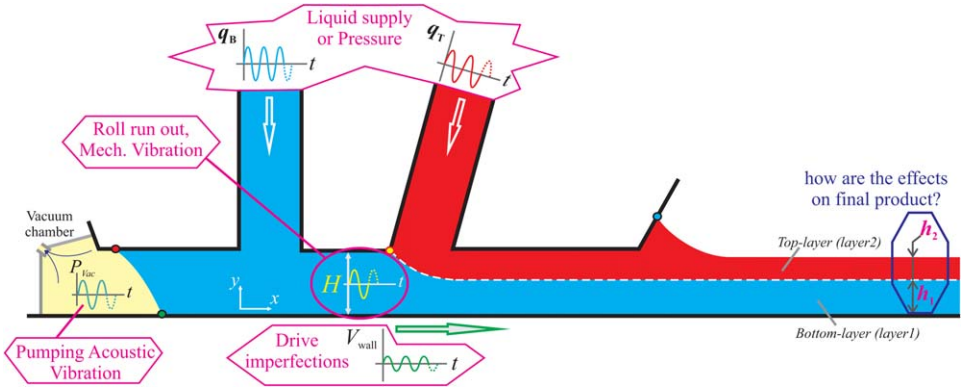

Figure 1. Sketch of two-layer slot coating process.

External disturbances are usually periodic variations on the coating gap, flow rate, vacuum pressure, and web speed. [Color figure can be viewed in the online issue, which is available at wileyonlinelibrary.com.]

viscosity difference, even in low Reynolds number flow, can generate instabilities along the interlayer, the so-called the interfacial mode in a plane Couette–Poisuille two-layer channel flow. Nam and Carvalho[9] used linear stability theory to analyze the stability of the interlayer in the downstream coating gap of a two-layer slot coating flow. The results show that stable flow is only possible with a thin top layer of a low viscosity liquid.

Products requiring extremely high-precision continuous coatings are common in the coating industry. Uniformity requirements are becoming even more severe as new products come into the market. Wet coating thickness variations higher than 1% are usually unacceptable. In a manufacturing plant, even in steady operation, there are inherent periodic disturbances at different frequencies that influence the uniformity of the coated layer. In the particular case of two-layer slot coating process, the external disturbances are usually periodic variations on the coating gap caused by roll run-out, mechanical vibration or nonuniform thickness of the substrate, periodic variation of the flow rate associated to fluctuations of the liquid supply or pressure, vacuum pressure variations related to acoustic vibration, and web speed variation.

Therefore, two-layer slot coating has to be designed not only based on the steady-state operation but also taking into account how the flow responds to ongoing external disturbances that are always present in a coating line. These disturbances may lead to thickness variation on each deposited liquid layer that may be unacceptable for product performance.

It is important to know how sensitive is the steady flow to these external disturbances, even if the flow is stable with respect to them and to determine, from the many different sets of operating conditions inside the coating window for a given product specification, which one will produce a more uniform final deposited layer. Once the flow response is known, the process may be designed to minimize the coating thickness variation.

Transient response analysis has been used to study different processes, including liquid coating. Van Addenyen[10] studied the response of coating flows to periodic infinitesimal disturbances and have shown that some disturbances may be amplified leading to large oscillations on the deposited liquid layer thickness. Transient flow response has also been used to determine the optimal baffle configuration that minimized sloshing in a tank.[11] Romero and Carvalho[12] solved the transient single-layer slot coating flow to determine the amplitude of the film thickness oscillation due to periodic variation on the flow rate and coating gap. The analysis showed the most dangerous frequencies for each type of disturbance and that the die lip configuration may be adjusted to reduce the sensitivity of the flow to periodic disturbances. The analysis was later extended by using the predicted film thickness amplitude as the objective function of a bound-constrained optimization problem to determine the values of vacuum pressure and coating gap, the two easiest parameters to control in a coating line that minimize the amplitude of the film thickness oscillation at a fixed web speed and flow rate.[13] Using a viscocapillary model, Tsuda[14] studied the use of active control with a flow feedback system coupled to film thickness sensors to reduce the amplitude of the film thickness oscillation.

Because of the presence of the interlayer and liquids with different viscosity, the dynamics of two-layer slot coating is very different than that of a single-layer flow. In this work, the transient response analysis is extended to two-layer slot coating flow to determine the amplitude of the oscillation of each individual coated layer associated with periodic perturbations on coating gap, web speed, and flow rate as a function of process conditions, die lip configuration, and frequency of the imposed disturbance.

Mathematical Model

The velocity $\mathbf{v}$ and pressure p fields of the transient, two-dimensional, incompressible flow of a Newtonian liquid are governed by the continuity and momentum conservation equations

$$\nabla \cdot \mathbf{v}=0; \tag{1}$$

$$\rho_i\left(\frac{\partial \mathbf{v}}{\partial t}+\mathbf{v}\cdot\nabla\mathbf{v}\right)-\nabla\cdot\mathbf{T}_i=0. \tag{2}$$

where ρ_i is the liquid density. The total stress tensor for Newtonian liquids is $\mathbf{T}_i=-p+\mu_i[\nabla\mathbf{v}+(\nabla\mathbf{v})^T]$ where μ_i is the liquid viscosity. Here, subscript i defines the two liquid phases, $i=T$ for the top layer and $i=B$ for the bottom layer. Because of the small dimensions of the flow, body forces are usually neglected in coating flows.

In a two-layer slot coating flow, the flow domain is bounded by inflow and outflow planes, solid walls and free

surfaces (gas–liquid interfaces), and the surface that separates the two liquids, the interlayer. The distance between the coating die and the moving substrate is called the coating gap. In the base die lip geometry, shown in Figure 1, the gap does not vary along the bead, that is, the upstream, mid, and downstream gaps are equal. The length of the mid and downstream die lip are equal to 0.5 and 1.25 mm, respectively. The imposed periodic oscillation of the gap $H(t)$ around the steady-state value H_0 is taken to be sinusoidal

$$H(t)=H_0+H_m \sin(\omega_H t), \tag{3}$$

where H_m is the amplitude of the imposed periodic disturbance and ω_H its angular frequency, which is related to the frequency f_H by $\omega_H=2\pi f_H$.

Boundary conditions are needed to solve the Navier–Stokes system. At the inflow planes, for example, at the die feeding slots, fully developed parallel rectilinear flow is assumed, where a Poiseuille velocity profile is prescribed as function of the flow rate per unit width of each layer $q_T(t)$ and $q_B(t)$. The imposed periodic oscillation on the flow rate of each layer is also taken to be sinusoidal, with a steady-state value q_{i0}, an amplitude q_{im} and an angular frequency ω_{qi}

$$q_i(t)=q_{i0}+q_{im} \sin(\omega_{qi} t). \tag{4}$$

The no-slip and no-penetration conditions applies along the die walls and the moving substrate

$$u=0, \quad v=0, \text{along the die walls.} \tag{5}$$

To study the effect of web speed oscillation, the imposed substrate velocity varies sinusoidally with time

$$u=V_0+V_m \sin(\omega_V t), \quad v=H_m \omega cos(\omega_H t). \tag{6}$$

V_0 is the steady-state substrate velocity. The imposed amplitude and angular frequency of the web speed periodic oscillation are V_m and ω_V, respectively. The vertical component of the substrate velocity is associated with the gap oscillation. For the cases at which the gap is constant, it is identically zero.

At the dynamic contact point, where the upstream meniscus meets the moving web, Navier-slip condition is used instead of no-slip condition and a dynamic contact angle θ_{dyn} is imposed

$$\frac{1}{\beta}\mathbf{t}_w \cdot (\mathbf{v}-V_0\mathbf{i})=\mathbf{t}_w \cdot (\mathbf{n}_w \cdot \mathbf{T}), \qquad \mathbf{n}_w \cdot \mathbf{n}_{fs}=\cos(\theta_{\text{dyn}}). \tag{7}$$

The upstream and downstream static contact lines are free to move along the upstream die lip and downstream die shoulder with a prescribed static contact angles θ_{si}

$$\mathbf{n}_w \cdot \mathbf{n}_{fs}=\cos(\theta_{si}). \tag{8}$$

Along the upstream and downstream gas–liquid interfaces, the traction in the liquid balances the capillary pressure and there is no mass flow rate across the interface. It is assumed that the gas viscosity is much smaller than the liquid viscosity, leading to vanishing shear stress along the gas–liquid interface

$$\mathbf{n}_{fs} \cdot \mathbf{T}=\sigma \frac{d\mathbf{t}_{fs}}{ds}-\mathbf{n}_{fs}p_0, \tag{9}$$

$$\mathbf{n}_{fs} \cdot (\mathbf{v}-\mathring{\mathbf{x}})=0, \tag{10}$$

where σ is the liquid surface tension, $\mathbf{t}_{fs}$ and $\mathbf{n}_{fs}$ are the local unit tangent and unit normal vectors to the free surface, $d\mathbf{t}_{fs}/ds$ represents the curvature of the meniscus, p_0 is the pressure of the gas, and $\mathring{\mathbf{x}}$ is the mesh velocity.[15] At the downstream free surface, the gas pressure is usually atmospheric, that is $p_0=P_{\text{atm}}$, and at the upstream free surface vacuum is applied to stabilize the coating bead, that is $p_0=P_{\text{vac}}$.

Like the gas–liquid interfaces, the posi tion of the interlayer is unknown *a priori*. To track its location, three conditions—force balance, no-penetration and velocity continuity—are to be satisfied along the interlayer

$$\mathbf{n}_I \cdot \mathbf{T}_T=\mathbf{n}_I \cdot \mathbf{T}_B+\sigma_I \frac{d\mathbf{t}_I}{ds}, \tag{11}$$

$$\mathbf{n}_I \cdot (\mathbf{v}_T-\mathring{\mathbf{x}})=\mathbf{n}_I \cdot (\mathbf{v}_B-\mathring{\mathbf{x}})=0, \tag{12}$$

$$\mathbf{t}_I \cdot \mathbf{v}_T=\mathbf{t}_I \cdot \mathbf{v}_B, \tag{13}$$

where $\mathbf{n}_I$ and $\mathbf{t}_I$ are the unit normal and tangent vectors to the interlayer. $\mathbf{v}_i$ and $\mathbf{T}_i$ are velocity and stress tensor for phase i, and σ_I is the interfacial tension. As in Eq. 10, $\mathring{\mathbf{x}}$ is the mesh velocity.

Initial condition is needed to solve the transient flow. In this work, the steady-state solution of the flow was used as the initial condition for the transient analysis. This initial condition had to be computed at each set of operating parameters. The periodic disturbances on each of the operating parameters lead to a transient response of the flow. The thickness of the each deposited liquid layer $h_i(t)$ varies periodically around the steady-state value $h_i(t=0)=h_{i0}=q_{i0}/V_0$ leading to a nonuniform film along the down-web direction

$$h_i(t)=h_{i0}+h_{im} \sin(\omega t+\phi_i), \tag{14}$$

The amplitude of the oscillation h_{im} and the phase lag of the thickness response ϕ_i are unknown and need to be determined for each condition. The ratio of the relative amplitude of the film thickness oscillation to the imposed operating parameters disturbance λ is called the amplification factor, defined as $\alpha_{ij}=[h_{im}/h_{i0}]/\lambda_j$. λ_j is associate with the source of the disturbances and represents the relative amplitude of the disturbed parameter. Here, subscript j defines different disturbances, $j=q_B$ for the bottom flow rate, $j=q_T$ for the top flow rate, $j=H$ for the gap, $j=$ Vac for the Vacuum pressure, and $j=V_W$ for the web speed oscillation. For example $\lambda_H=H_m/H_0$.

Two-layer slot coating can be used for different applications, spanning a broad range of parameters, from very viscous non Newtonian dispersions to low viscosity Newtonian liquids; from very thin films to relatively thick layers. The operating parameters of two-layer slot coating process, their respective range covering different applications and the values considered as base case in this analysis are presented in Table 1. In the base case considered here, the two liquid layers have the same viscosity and surface tension. The static contact angle between the downstream free surface and the die shoulder was larger than the contact angle between the upstream meniscus and the die lip. In some applications, the die surface is treated to avoid or minimize wetting of the die shoulder. The process variables can be grouped in the downstream parameters listed in Table 2. The values of the dimensionless number for the base case are also shown. They are close to those encountered in two-layer slot coating of pressure sensitive adhesives.[16]

Solution Method

Flows with free surfaces and interlayer give rise to a free-boundary problem. The flow domain is unknown a priori,

Table 1. Parameters for a Typical Two-Layer Slot Coating

Operating Parameters				
Parameter	Unit	Symbol	Range	Base Case
Gap width	μm	H	50–300	250
Web speed	ms^{-1}	V_w	0–5	1
Pressure difference	kPa	P_{vac}	0–10	2
Dynamic contact angle	°	θ_d	140–160	140
Upstream static contact angle	°	θ_{s-u}	5–90	60
Downstream static contact angle	°	θ_{s-d}	5–90	90
Interfacial tension	mN/m	σ_I	0–1	1
Density	kgm^{-3}	ρ_T, ρ_B	900–1300	$\rho_T=\rho_B=1200$
Viscosity	mPa.s	μ_T, μ_B	0.5–1000	$\mu_T=\mu_B=25$
Surface tension	mN/m	σ_T, σ_B	20–60	$\sigma_T=\sigma_B=60$
Film thickness	μm	h_T, h_B	20–150	$h_B=125$, $h_T=62.5$

and it is part of the solution. To solve a free-boundary problem by means of standard techniques for boundary value problems, the set of differential equations and boundary conditions posed in the unknown physical domain have to be transformed to an equivalent set defined in a known, fixed computational domain. This transformation is made by a mapping $\mathbf{x}=x(\boldsymbol{\xi})$ that connects the two domains. The physical domain is parameterized by the position vector $x=(x,y)$ and the reference domain by $\boldsymbol{\xi}=(\xi,\eta)$.[15]

The mapping used here is the one described previously.[17] The inverse mapping is governed by a system of elliptic differential equations identical to those encountered in the dilute regime of diffusional transport

$$\nabla \cdot D_\xi(\xi,\eta)\nabla\xi=0, \nabla \cdot D_\eta(\xi,\eta)\nabla\eta=0. \tag{15}$$

D_ξ and D_η are mesh diffusivities which control the steepness of gradients in the node-spacing by adjusting the potentials ξ and η. Curves of constant ξ and η define the boundaries of elements used to describe the domain. The cross point of these curves sets the position of a node. Boundary conditions are needed to solve the second-order differential equations (15). Solid walls and inflow and outflow planes are described by the function that defines their geometry and nodes were distributed along them by a specified stretching function. The location of the free surfaces and interlayer are implicitly determined by the corresponding kinematic conditions Eqs. 10 and 12. The discrete version of the mapping equations is generally referred to as mesh generation equations. Detailed procedure and boundary conditions for mesh equation are discussed in de Santos.[17]

In transient problems, the frame of reference lies across the space-time domain for which the physical grid points are constantly updated in time. Therefore, time derivative at fixed Eulerian locations in space needs to be transformed to time derivative at fixed isoparametric coordinates. The time derivative of the nodal position, that is, the mesh velocity, needs to be considered in the momentum equation[16]

Table 2. Dimensionless Parameters

Dimensionless Parameters		
Group	Definition	Base Case
Reynolds number	$Re=\rho V_w H/\mu$	12
Capillary number	$Ca=\mu V_w/\sigma$	0.42
Vacuum Pressure	$\text{Vac}=P_{vac}H/\sigma$	6.25
Bottom-layer thickness ratio	$G_B=H/h_B$	2
Top-layer thickness ratio	$G_T=H/h_T$	4
Viscosity ratio	$\kappa=\mu_B/\mu_T$	1

$$\rho_i[\mathring{v}+(\mathbf{v}-\mathring{\mathbf{x}})\cdot\nabla\mathbf{v}]-\nabla\cdot\mathbf{T}_i=0, \tag{16}$$

The system of governing equations together with the appropriate boundary conditions and initial condition was solved by Galerkin's method with quadrilateral finite elements. Details on the finite element discretization are discussed by Romero and Carvalho.[12]

Once all the variables are represented in terms of the basis functions, the system of partial differential equations reduces to a set of ordinary differential and algebraic equations that describe the evolution of the coefficients with time

$$\mathbf{R}(\mathbf{u},\dot{\mathbf{u}},\mathbf{f}(t))=0, \tag{17}$$

where $\mathbf{R}$ is the set of weighted residual equations, $\mathbf{u}$ is the vector of basis functions' coefficients, $\dot{\mathbf{u}}$ is their time derivatives, and $\mathbf{f}$ a vector that contain all the input parameters (physical properties, geometry of the flow and boundary condition information).

As mentioned before, the initial condition of the transient flows related to the imposed oscillation on the different operating variables was the steady-state flow without any imposed oscillation. Therefore, the first step of the analysis was the solution of the steady-state flow. The system of ordinary differential-algebraic equations is reduced to simultaneous algebraic nonlinear equations for the coefficients of the basis functions of all the fields

$$\mathbf{R}(\mathbf{u},\mathbf{f_0})=0, \tag{18}$$

which was solved by Newton's method that requires the evaluation of the Jacobian matrix. The vector $\mathbf{f_0}$ contains the input parameters of the steady-state flow.

The temporal discretization of the set of ordinary differential-algebraic equations follows the first-order fully implicit Euler method. A mesh with 1120 elements (22,228 degrees of freedom) as shown in Figure 2, was considered satisfactory and was used to obtain the solutions reported here. A time step of $\Delta t \approx 70\omega$ was adopted in all computations, that is, 140 time steps were used per cycle of the imposed periodic perturbation.

Results

In a coating line, operating parameters oscillations come from many different sources, each of them with a characteristic frequency. Figure 3 summarizes the frequency range of the most common disturbances.[14] For all the disturbances considered here, the range explored was from $0.01 < f < 1000\text{Hz}$.

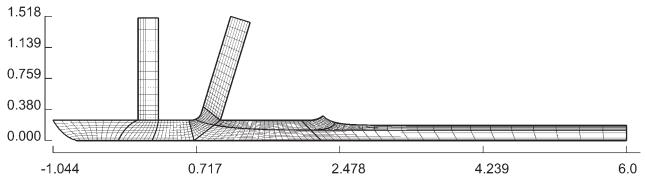

Figure 2. Finite element mesh used in the analysis.

Quadrilateral mesh with 1120 elements and 22,228 degrees of freedom.

A large number of die lip configurations has been disclosed in the patent literature claiming improvement on the production speed and quality of the coated film. The effect of die lip configuration in the amplitude of the film thickness oscillation related to different disturbances is analyzed here by comparing transient flow predictions using three different configurations considered by Sartor et al.,[4,15] shown in Figure 4: The base case (B) with a constant gap along the bead; the underbite configuration (U), at which the die lips are mounted with an offset such that the upstream gap is smaller than the midgap, which is smaller than the downstream gap; and the tilted die configuration (T) that is simply the underbite configuration tilted by an angle of 3°.

The effect of static contact line boundary condition on the dynamic response

An approximation largely used in coating flow analysis is to consider static contact lines pinned at sharp corners of coating dies as sketched in Figure 5a. This simplification easies the requirements on the mesh generation and element deformation and leads to accurate steady-state results.[12–14]

However, it is well known that the meniscus can climb along the die shoulder or recede into the bead along the downstream die at certain operating conditions. Kapur[18] and Romero and Carvalho[19] solved steady-state slot coating flows considering that the downstream meniscus was free to climb the die surface. Nam and Carvalho[7] considered two-layer slot coating flow with both the downstream contact line and the interlayer separating point free to move along the die surface as sketched in Figure 5b. The goal was to determine the undesirable conditions at which the separating point invades the mid die lip. The effect of the movement of the static contact line on the transient response of the flow is not known and is investigated here for the base die configuration B. The main goal of this comparison is to evaluate the accuracy of the predictions available in the literature for fixed contact line.

Figure 6 shows the amplification factor for each layer as a function of the imposed frequency of the bottom-layer flow rate oscillation for the two different boundary condition: pinned contact lines (circles) and free contact lines (triangles). Predictions were obtained at the conditions shown in

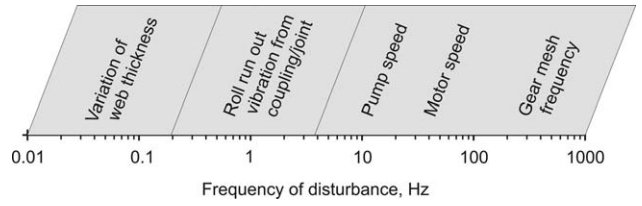

Figure 3. Frequency of different disturbances that occur in slot coating process.

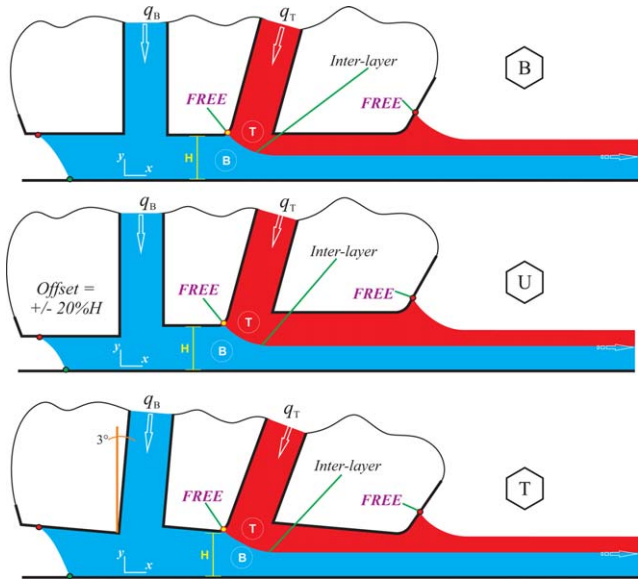

Figure 4. Sketch of different die lip configurations considered: Base case B, underbite U, and tilted T.

[Color figure can be viewed in the online issue, which is available at wileyonlinelibrary.com.]

Table 1. The amplitude of the perturbation was set at 10% of the steady-state value $q_{Bm}=0.1q_{B0}$. At very low frequency, the amplification factor associated with the top-layer oscillation virtually vanishes while the amplification factor of the bottom layer is close to unity. This behavior is expected as a quasi steady state is reached as the perturbation frequency approaches zero. In steady state, the top-layer thickness is not a function of the bottom-layer flow rate and the bottom-layer thickness is directly proportional to it. As the frequency increases, the amplification factor of the top layer rises, until reaching a maximum value close to a frequency of 200 Hz. A second harmonic is observed at a frequency close to 750 Hz. The amplification factor of the bottom-layer thickness remains close to one for frequency below 10 Hz. Above this value, it falls monotonically.

The effect of the static contact lines boundary condition is only evident for frequency higher than 10 Hz and on the amplification factor of the top layer. The predictions using

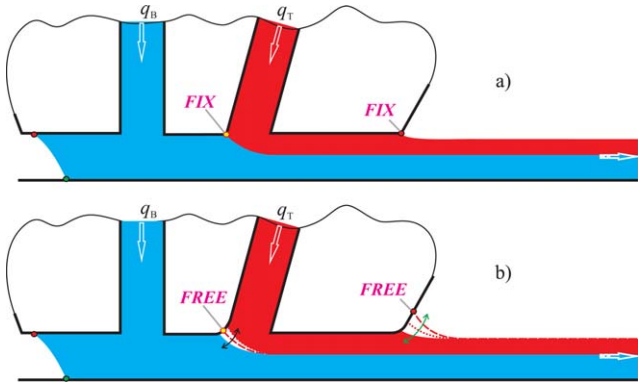

Figure 5. Boundary condition at the separation point and downstream static contact line: a) pinned and b) unpinned.

[Color figure can be viewed in the online issue, which is available at wileyonlinelibrary.com.]

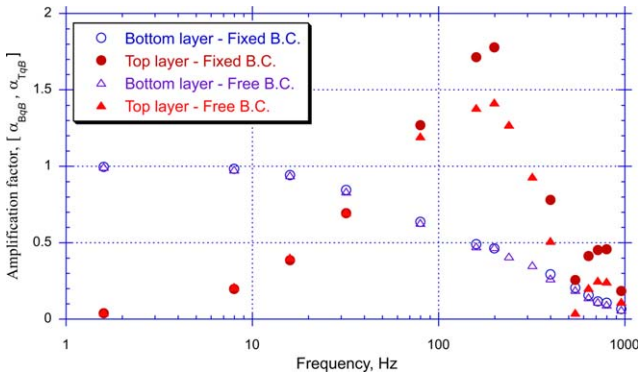

Figure 6. Effect of static contact line boundary condition on the amplification factor related to bottom-layer flow rate oscillation.

Predictions obtained with the base die lip configuration B. [Color figure can be viewed in the online issue, which is available at wileyonlinelibrary.com.]

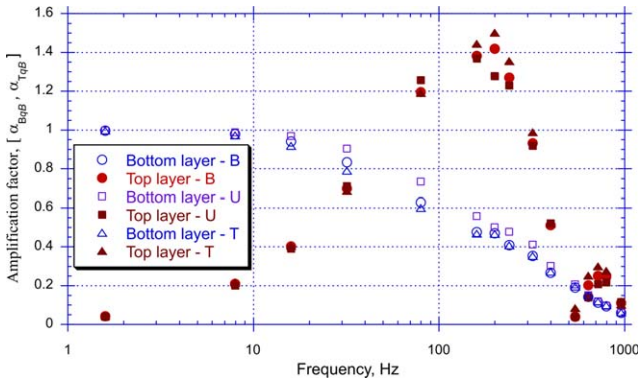

Figure 8. Amplification factor of both layers associated to bottom-layer flow rate oscillation for the three different die lip configuration.

[Color figure can be viewed in the online issue, which is available at wileyonlinelibrary.com.]

the fixed static contact lines boundary condition led to larger amplitudes on the top-layer film thickness oscillation. The maximum amplification factor (at $f \approx 200$ Hz) is 1.8 for the fixed static contact line case and 1.4 for the free contact line condition. When the contact line is free to move along the die surfaces, the flow perturbations can be accommodated by the movement of the contact line, yielding smaller amplitude oscillation of the meniscus. The boundary condition had no effect on the bottom-layer amplitude. This behavior can be explained by the fact that even if it is free to move along the midlip die surface, the separating contact line position remains more or less fixed, if the bottom-layer flow rate is above 1/3 of the gap.[7]

The flow response using both boundary conditions when the vacuum pressure is perturbed is shown in Figure 7. The amplitude perturbation was again set at 10% of the steady-state value, for example, $P_{\text{vacm}}=0.1P_{\text{vac0}}$. At low frequencies, the amplification factor of both layers approach zero. This behavior is expected; at steady state, the film thickness should be independent of the vacuum pressure. As the perturbation frequency rises, both amplification factors increase, reaching a maximum at a frequency close to 100 Hz for the bottom layer and 200 Hz for the top layer. The top layer is more sensitive to vacuum fluctuations than the bottom layer, reaching a maximum amplification factor close to 1. The maximum amplification factor of the bottom layer is close to 0.35. Again, the effect of the static contact line boundary condition is only evident for frequency higher than 10 Hz, and the pinned contact line led to higher amplitude of top-layer film thickness oscillation.

In summary, the transient behavior of the flow is not strongly affected by the static contact line boundary condition. The dependence of the amplification factors of both layers on the imposed disturbance frequency follows the same trend. However, the fixed contact line position boundary condition led to top-layer film thickness amplitude larger than that obtained with the slipping contact line boundary condition. From this point on, all the predictions were obtained assuming that the contact lines are free to move along the die surfaces.

Transient response: Sensitivity to operating parameter disturbances

The transient response of the flow to different operating parameter disturbances is analyzed. The results are presented in terms of the amplification factor for both layers. Predictions were obtained at the conditions listed in Table 1.

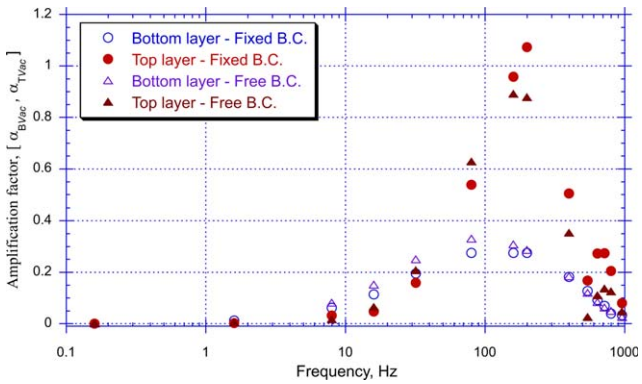

Figure 7. Effect of static contact line boundary condition on the amplification factor related to vacuum pressure oscillation.

Predictions obtained with the base die lip configuration B. [Color figure can be viewed in the online issue, which is available at wileyonlinelibrary.com.]

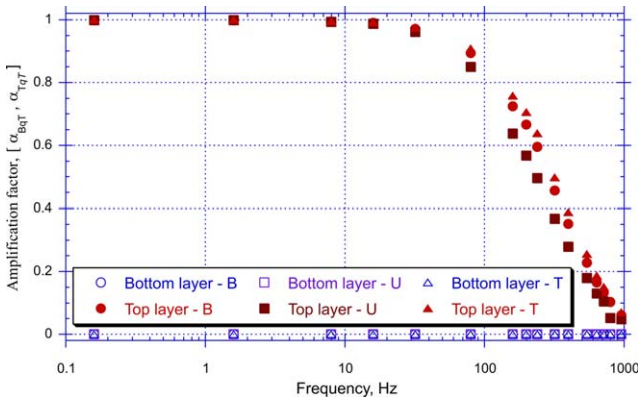

Figure 9. Amplification factor of both layers associated to top-layer flow rate oscillation for the three different die lip configuration.

[Color figure can be viewed in the online issue, which is available at wileyonlinelibrary.com.]

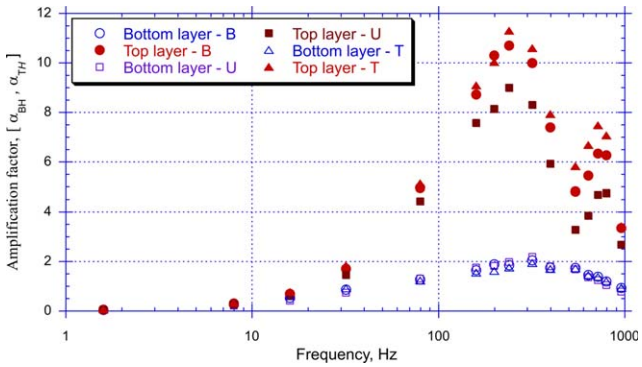

Figure 10. Amplification factor of both layers associated to coating gap oscillation for the three different die lip configuration.

[Color figure can be viewed in the online issue, which is available at wileyonlinelibrary.com.]

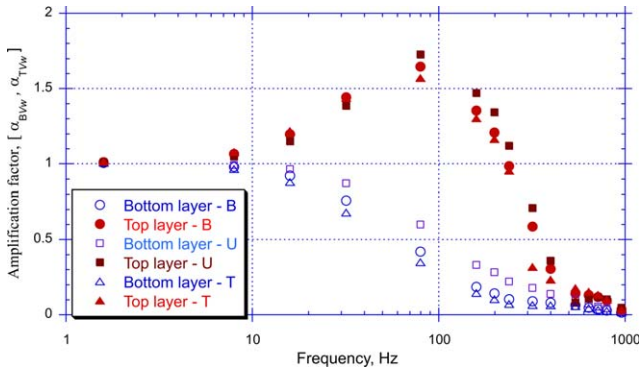

Figure 12. Amplification factor of both layers associated to web speed oscillation for the three different die lip configuration.

[Color figure can be viewed in the online issue, which is available at wileyonlinelibrary.com.]

The amplification factor of both layers for the three die configurations associated with bottom-layer flow rate perturbation are presented in Figure 8. As discussed before, at low frequencies, a quasi steady-state condition is approached and the bottom-layer thickness h_B is proportional, and the top-layer thickness h_T is independent of the imposed bottom-layer flow rate q_B. Consequently, the amplification factor of the bottom layer is $\alpha_{qB} \approx 1$ and that of the top layer is $\alpha_{qT} \approx 0$. As the frequency rises, the diffusion of momentum occurs in a time scale comparable to the imposed perturbation and the amplification factor of the bottom layer decrease monotonically as the frequency rises. The amplitude of the top-layer oscillation rises with frequency until reaching a maximum $\alpha_{qT} \approx 1.4$ for the base die configuration (B), $\alpha_{qT} \approx 1.5$ for the tilted configuration (T), and $\alpha_{qT} \approx 1.37$ for the underbite die configuration (U). The frequency at which the maximum amplification factor occurs (natural frequency) is close to 200 Hz. Above this value, the amplification factor falls until a second resonance peak appears at $f \approx 750$Hz. The die lip configuration has a weak effect on the transient response of the flow related to bottom-layer flow rate oscillation. The predictions show that operating the pumping system at high frequency minimizes the film thickness oscillation of both layers for all the die lip configurations explored.

Comparing the two-layer slot coating response to the predictions of single-layer transient analysis presented by Romero and Carvalho,[12] the bottom-layer behavior is similar to flow rate disturbance and the top-layer response is similar to gap disturbance in single-layer coating.

Figure 9 presents the transient response for the three die configurations related to top-layer flow rate oscillation. The amplitude of the perturbation was set at $q_{1m}=0.1q_{10}$. The effect on the bottom layer is very weak, $\alpha_{qB} \approx 0$ for the entire frequency range explored. The top-layer amplification factor is close to $\alpha_{qT} \approx 1$ at low frequency and falls monotonically for $f > 10$ Hz. The underbite configuration U led to smaller amplification factors. Again, oscillations from the pumping system are damped if it is operated at high frequencies.

Periodic variations of the coating gap can be associated with roll run-out, mechanical vibration or web thickness variations. The transient response of the flow to gap oscillation is shown in Figure 10. The amplitude of perturbation was set at 1% of the steady-state value $h_m=0.01H_0$. At low frequency, the amplification factor of both layers approach zero. In quasi steady state, the thickness of each layer is independent of the coating gap. As the disturbance frequency increases, the amplitude of the film thickness oscillation rises

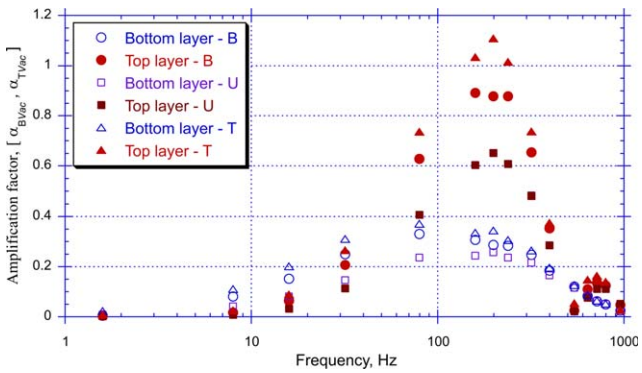

Figure 11. Amplification factor of both layers associated to vacuum pressure oscillation for the three different die lip configuration.

[Color figure can be viewed in the online issue, which is available at wileyonlinelibrary.com.]

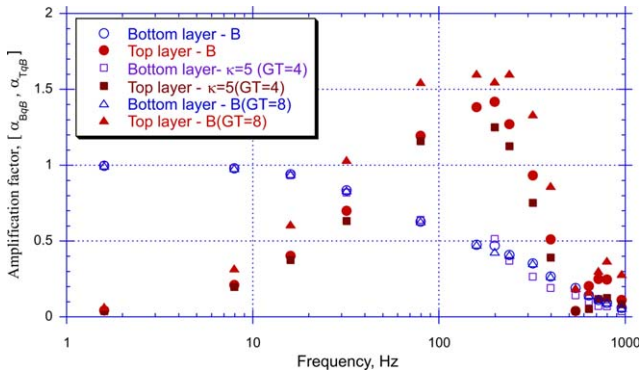

Figure 13. Effect of viscosity ratio κ and top-layer thickness G_T on the amplification factor associated to bottom-layer flow rate oscillation.

[Color figure can be viewed in the online issue, which is available at wileyonlinelibrary.com.]

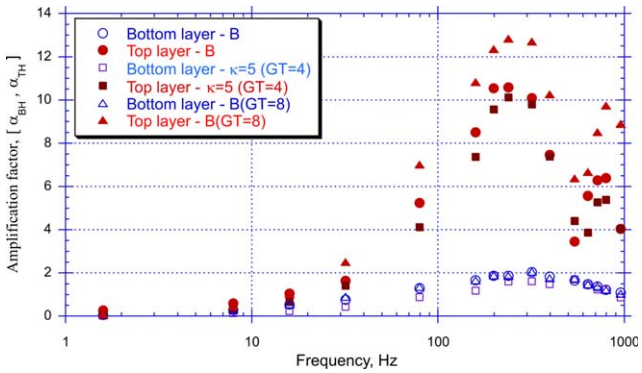

Figure 14. Effect of viscosity ratio κ and top-layer thickness G_T on the amplification factor associated to coating gap oscillation.

[Color figure can be viewed in the online issue, which is available at wileyonlinelibrary.com.]

until reaching the first peak at a frequency close to 200 Hz for the top layer and 300 Hz for the bottom layer. The resonance frequency is associated with the ratio of characteristic time scales or perturbation and momentum diffusion through each layer.[12]

In two-layer slot coating, the film thickness is extremely sensitive to gap disturbances. The maximum amplification factor is above 1 for both layers, the relative amplitude of the film thickness oscillation is larger than the relative amplitude of the gap perturbation. The maximum amplification factor for the bottom-layer thickness is close to $\alpha_{BH} \approx 2$ and for the top-layer thickness is approximately to $\alpha_{TH} \approx 11$. A 0.5 μm roll runout in a gap of $H_0 = 100$ μm may lead to a top-layer film thickness fluctuation of approximately 1.5 μm for a top-layer thickness of 25 μm, which may be unacceptable in many applications. The underbite die lip configuration U led to the lowest top-layer amplification factor over the entire range of frequency explored. The effect of the die configuration on the bottom-layer response was weak.

The effect of vacuum pressure disturbance on the amplitude of the film thickness oscillation is shown in Figure 11. As before, the amplitude of the periodic vacuum pressure disturbance was set at $P_{\text{vacm}} = 0.1 P_{\text{vac0}}$. In steady state, the film thickness is independent of vacuum pressure, and therefore, at low frequency, the amplitude of the film thickness oscillation approaches zero. As the disturbance frequency rises, the amplification factor rises until reaching the first peak at a frequency close to 200 Hz for the top layer and 100 Hz for the bottom layer. As in the case of gap disturbance, the top layer is more sensitive than the bottom layer; the amplification factor of the top layer is larger than the bottom layer. Again, the underbite die lip configuration U led to the lowest top-layer amplification factor over the entire range of frequency explored.

Figure 12 presents the transient response for the three die configurations related to web speed oscillation. As in the previous cases, the amplitude of perturbation was set at 10% of the steady-state value $V_m = 0.1 V_{w0}$. At low frequency, the amplification factor of both layers is equal to 1. At steady state, the film thickness is directly proportional to the web speed. For $f > 10$ Hz, the oscillation on the bottom-layer thickness is damped and the amplification factor falls monotonically as frequency rises. The transient response of the top layer is completely different. The amplification factor first rises until reaching a maximum value at $f \approx 100$Hz and then falls to almost zero at $f \approx 1000$Hz. For web speed disturbance, the tilted die configuration T led to the smallest amplification factors. The converging channel creates an adverse pressure gradient that promotes a stronger disturbance on the upstream meniscus position, reducing the film thickness oscillation.

Effect of the viscosity ratio and the top-layer feed rate

The dynamic response of the flow is a function of the steady-state operating parameters. The effect of viscosity ratio and top-layer thickness on the amplification factor related to bottom-layer flow rate disturbance is analyzed for the base die configuration B.

Figure 13 compares the amplification factor obtained at viscosity ratio $\kappa = 1$ and gap to top-layer thickness ratio $G_T = 4$, previously presented in Figure 8, to the predictions obtained with a less viscous top-layer liquid ($\kappa = 5$) and thinner top layer ($G_T = 8$). The amplification factor associated with the bottom-layer oscillation does not change much with the top-layer viscosity and thickness. The top-layer disturbance amplitude is higher for thinner top layer and lower for less viscous top-layer thickness.

The amplification factors associated with coating gap oscillation are shown in Figure 14. Again, the bottom-layer disturbance was not strongly affected by changes on the top-layer conditions, that is, viscosity and thickness. As in Figure 13, thinner top layer let to higher amplitudes and less viscous top layer led to lower amplification factors.

Final Remarks

The transient response of two-layer slot coating flow to different periodic disturbances on operating parameters were analyzed here by solving the momentum and continuity equation system for transient, two-dimensional, free surface flows.

The results clearly show that small perturbations on the operating parameters can lead to large oscillation on the thickness of both layers. The amplitude of the oscillation is a strong function of the frequency of the imposed disturbance. Frequencies close to the resonance values should be avoided in operation. This should be taken into account on the design of new coating lines.

In general, the top layer is more sensitive to the operating parameters disturbances. The most dangerous disturbance that leads to the highest amplification factors, is the perturbations on the coating gap, usually associated with mechanical vibration of the coating head or roll run-out.

The amplitude of the film thickness oscillation can be reduced by changing the die lip configuration, viscosity ratio, and wet thickness of the films. For the range explored here, the underbite configuration reduced the amplitude of the oscillation for most of the disturbances considered in the analysis.

Acknowledgments

This work was funded by CNPq (Brazilian Research Council) and by the Industrial Partnership for Research in Interfacial and Materials Engineering (IPRIME) of the University of Minnesota.

Literature Cited

1. Beguin AE. Method of coating strip material. U.S. Patent 2681294, 1954.

2. Russell TA. Multiple coating apparatus. U.S. Patent 2761418, 1956.
3. Musson LC. *Two-Layer Slot Coating*. Ph.D. Thesis. University of Minnesota, MN, 2001.
4. Sartor L, Huff S, Kishi CN. Method for multilayer coating using pressure gradient regulations. U.S. Patent 5728430, 1998.
5. Taylor SD, Hrymak AN. Visualization and flow simulation of a two-slot coater. *Chem Eng Sci*. 1990;54:909–918.
6. Cohen D. Two-layer slot coating flow visualization and modelling. Masters thesis. University of Minnesota, MN, 1993.
7. Nam J, Carvalho MS. Mid-gap invasion in two layer slot coating. *J Fluid Mech*. 2009;631:397–417.
8. Yih C. Instability due to viscosity stratification. *J Fluid Mech*. 1967; 27:337–351.
9. Nam J, Carvalho MS. Linear stability analysis of two-layer rectilinear flow in slot coating. *AIChE J*. 2010;56(10):2503–2512.
10. Van Abbenyen W, Christodoulou KN, Scriven LE. Frequency response of coating flow. University of Minnesota Supercomputer Institute Report UMSI89/40, 1989.
11. Cho JR, Lee SY. Dynamic analysis of baffled fuel-storage tanks using the ALE finite element method. *Int J Numer Methods Fluids*. 2003;41:185–208.
12. Romero OJ, Carvalho MS. Response of slot coating flows to periodic disturbances. *Chem Eng Sci*. 2008;63:2161–2173.
13. Perez EB, Carvalho MS. Optimization of slot coating process: minimizing the amplitude of film thickness oscillation. *J Eng Math*. 2010;71:97–108.
14. Tsuda T. Dynamic response analysis and control of slot coating. *J Fluid Sci Technol*. 2009;4(3):735–745.
15. Christodoulou KN, Scriven LE. Discretization of free surface flows and other moving boundary problems. *J Comput Phys*. 1992;99:39–55.
16. Sartor L, Huff S, Kishi CN. Method for multilayer coating using viscosity adjustment technique. U.S. Patent 5962075, 1999.
17. de Santos JM. Two-phase cocurrent downflow through constricted passages. Ph.D. Thesis. University of Minnesota, MN, 1991.
18. Kapur N. Flow phenomena in fixed-gap and gravure roll coating systems. Ph.D. Thesis University of Leeds, 1999.
19. Romero OJ, Scriven LE, Carvalho MS. Effect of curvature of coating die edges on the pinning of contact line. *AIChE J*. 2006;52(2): 447–455.

Manuscript received Oct. 3, 2014, and revision received Nov. 21, 2014.